General Disclaimer

One or more of the Following Statements may affect this Document

- This document has been reproduced from the best copy furnished by the organizational source. It is being released in the interest of making available as much information as possible.

- This document may contain data, which exceeds the sheet parameters. It was furnished in this condition by the organizational source and is the best copy available.

- This document may contain tone-on-tone or color graphs, charts and/or pictures, which have been reproduced in black and white.

- This document is paginated as submitted by the original source.

- Portions of this document are not fully legible due to the historical nature of some of the material. However, it is the best reproduction available from the original submission.

NASA Technical Memorandum 78998

WIND TUNNEL TESTS OF A BLADE SUBJECTED TO MIDCHORD TORSIONAL OSCILLATION AT HIGH SUBSONIC STALL FLUTTER CONDITIONS

D. R. Boldman and A. E. Buggele
Lewis Research Center
Cleveland, Ohio

October 1978

SUMMARY

A novel mechanical drive system for oscillating blades in a wind tunnel at frequencies up to 767 hertz and amplitudes of $\pm 1.2^{\circ}$ is described. High-speed motion pictures of Schlieren images of the flow over a double-circular arc blade oscillating in harmonic motion about the midchord revealed rather extensive shock patterns at a nominal free stream Mach number of 0.7, a mean angle of attack of 4°, and reduced frequency of about 0.7. A phase lag resulting from the slow response of the flow to the motion of the blade increased with increasing reduced frequency. This phase lag, based on the difference between the time the blade attained its maximum angle of attack and the time required for the normal shock to reach its extreme downstream position, was nominally 100° at the above conditions.

E-9782

INTRODUCTION

Some four or five types of flutter have been identified in the operation of turbomachinery. One type, which has been particularly difficult to model in analytical prediction methods, is a subsonic torsional stall flutter which occurs near the compressor surge line. This type of flutter is believed to be associated with intermittent flow separation on the blade and an aerodynamic lag between the flow response and the high frequency oscillatory motion of the blade (refs. 1 to 5). The aerodynamic modeling of the stall flutter at high subsonic Mach numbers is further complicated by the presence of unsteady shock waves in the blade passages.

One method for studying this type of flutter is by observing the flow in a two-dimensional cascade wind tunnel while simulating the flow conditions and blade motion associated with the flutter. Data obtained in this manner would provide a guide for the selection of an appropriate flow model and serve to verify analytical results. In order for this flutter cascade to be effective, it is necessary to establish (1) that highly loaded blades can be driven at frequencies in the range of 500 to 800 hertz at nominal amplitudes of $\pm 1^{\circ}$, and (2) that a suitable flow visualization system, compatible with the drive system and flow conditions, can be developed. This report describes a pilot study in which a single airfoil is driven at the required conditions and a flow visualization

technique is applied. The blade drive mechanism and flow visualization system are described and some of the flow visualization results are presented.

The tests were performed in the NASA Lewis Research Center's 10- by 25-centimeter wind tunnel at free-stream Mach numbers of about 0.7 corresponding to a nominal Reynolds number based on blade chord of 1×10^6. Although free-stream Mach numbers were subsonic, local Mach numbers near the leading edge of the loaded blade exceeded Mach 1 as evidenced by the formation of shock waves.

SYMBOLS

c	blade chord
$\overline{e^2}_{1,2,\ldots,n}$	mean-square amplitude of n^{th} harmonic of blade motion
f	blade oscillatory frequency
M_∞	free-stream Mach number
M_{ref}	reference Mach number for the wind tunnel
Re_c	Reynolds number based on blade chord
t	time
U_∞	free-stream velocity
α	instantaneous angle of attack
$\overline{\alpha}$	mean angle of attack
θ_o	torsional amplitude
Φ	phase lag
Ψ	harmonic distortion function
ω	angular frequency
Ω	reduced frequency
Subscripts:	
m	maximum value
s	associated with maximum downstream normal shock position

APPARATUS

Wind Tunnel

The blade flutter tests were performed in the LeRC 10- by 25-centimeter wind tunnel shown schematically in figure 1. Room air entered the plenum and expanded through the 144-centimeter-long constant area test section into a diffuser and exhaust header maintained at a pressure of 3.0 N/cm^2. Flow rates were established by means of two valves located downstream of the diffuser. These valves were arranged with the smaller valve forming a bypass circuit around the larger valve. The majority of tests were performed at a nominal free-stream Mach number of 0.7.

Blade

The blade (shown in fig. 2) was a two-dimensional uncambered double-circular arc configuration having a chord of 7.62 centimeters and a span of 9.60 centimeters. The blade radius of curvature was 27.4 centimeters yielding a maximum thickness of 0.58 centimeter or a thickness-to-chord ratio of 0.076. The blade, which was fabricated from titanium containing 6 percent aluminum and 4 percent vanadium, was supported by two trunnions with the centerline located at midchord as shown in figure 2. The driven shaft had a diameter of 1.91 centimeters whereas the freely supported shaft had a diameter of 0.95 centimeter. The large shaft contained a 2.22-centimeter-diameter stainless steel shrink-fitted sleeve machined to match a bushing in the wind tunnel side wall. Fillets were provided at each trunnion as shown. The blade and trunnions were machined from a single piece of stock.

Blade Installation

The blade was installed near the centerline of the wind tunnel and was positioned so that the leading edge was 47.0 centimeters downstream of the entrance station where the tunnel cross section became constant. The blade was first inserted into a side plate containing a 0.64-centimeter-thick mirror which was part of a Schlieren optical system (fig. 1). A bronze alloy bushing contained an "O" ring groove as well as three equally spaced helical grooves which provided a lubrication path for the large trunnion. Initial tests with an oil im-

pregnated bushing and O-ring resulted in a slight leakage of the lubricant into the low-pressure test section. Although this leakage was small, it was sufficient to cause a foggy deposit on the mirror and, consequently, partially obscured the Schlieren image downstream of the trunnion. Incorporation of the nonporous bronze alloy bushing eliminated this leakage problem.

A wind tunnel side plate containing an optical quality glass window was installed at the freely supported end of the blade. A bronze alloy bushing with eight partial slits was pressed into the glass window to provide support for the small trunnion.

The limitation in the region of flow visualization over the blade surface in this type of installation is governed by the large trunnion and the size of the hole in the mirror required to accommodate the fillet (refer to fig. 2). In order to maximize the flow visualization in the blade midchord region, a countersunk hole resembling an elliptical rather than a circular hole was inserted in the mirror. This shape of hole also minimized the interference to the flow in the vicinity of the large trunnion.

Blade Drive System

Electromagnetic and mechanical drive systems have been used for the torsional oscillation of airfoils in wind tunnels as reported, for example, in references 6 and 7, respectively. Electromagnetic drive systems have the capability of generating torsional oscillatory motion at controlled high frequencies (hundreds of hertz); however, in these systems the amplitude of the motion decreases with increasing frequency. Mechanical drive systems of the type described in references 2 and 6, provide absolute control of both frequency and amplitude; however, this type of system is usually limited to lower operating frequencies (perhaps up to 100 Hz).

In the present investigation, control of the oscillatory amplitude as well as the frequency was desired; therefore, a special high-speed drive system was developed for this purpose. This drive system, which is described below, permitted control of both frequency and amplitude at oscillatory frequencies in the hundreds of hertz for steady-state flutter simulation of 10- to 20-second duration.

The blade was oscillated in a controlled fashion at frequencies which were limited only by the onset of appreciable twisting of the blade (at about 750 Hz). Run times were nominally 30 seconds with 10 to 20 seconds at steady oscillatory

frequencies. The oscillatory motion was provided by a mechanical drive system powered by a 7.5-horsepower electric motor as shown in figure 3. In this type of system, frequency amplification for each blade was attained from a female barrel cam having a 3-cycle, 1.27-centimeter-wide by 0.762-centimeter-deep sinusoidal groove machined in the surface. A close-coupled connecting arm and button follower transmitted 3 cycles of oscillatory harmonic motion to the blade for each revolution of the cam. The blade oscillatory frequency was changed by altering the pulley size on the constant speed motor or on the cam shaft. The pulleys were connected by a special 2.54-centimeter-wide endless belt consisting of layers of plastic-coated textile fabric, a polyester tension member, and a leather friction surface. Amplitude control was achieved by the cam groove design. The cam and follower were immersed in a multiviscosity 85W-140 high-performance gear lubricant to minimize wear.

The connecting arm between the cam and blade trunnion was 7.62-centimeter-long and fabricated from titanium. A hexagonal hole and clamping arrangement were used to couple the blade and connecting arm. In this type of arrangement, the blade angle of attack was set by displacing the cam shaft along its axis.

The cam and button follower were fabricated from 440C stainless steel, heat treated to obtain a cam hardness of 60 Rockwell C and a yield strength of 190 000 N/cm^2. The button hardness was approximately 5 Rockwell less than the cam so that the major wear would be incurred in the button rather than the cam. The button could be rotated to four different positions prior to removal, therefore minimizing the maintenance time. However, cam and button wear problems, which were of concern in initial tests of the drive system, were virtually eliminated by incorporating the 85W-140 high-performance gear lubricant rather than lighter-weight oils which were used in earlier tests of the drive system. For example, an initial clearance of 0.0018±0.0005 centimeter between the cam and button follower increased by only 0.0003 centimeter in a total of 40 runs of approximately 30- to 40-second duration, frequencies of 500 to 767 hertz, and a blade oscillatory amplitude of $\pm 1.2^{\circ}$ about the mean angle of attack.

Another significant factor that increased the drive system reliability was the prevention of minute air bubbles within the gear lubricant at cam shaft rotational speeds up to 16 000 rpm. At high rotational speeds with large displacement female barrl cams, the cam shaft can execute a whipping motion

which draws air into the enclosure at the shaft seals. The entrained air forms minute bubbles which effectively reduces the lubricity of the gear lubricant, thereby increasing button wear. With increasing cam-follower wear the harmonic motion becomes altered by what is commonly called a pulse or "jerk". In reference 8 this pulse is defined as the instantaneous time rate of change of acceleration of the cam follower. In references 9 and 10 cam-follower backlash or crossover shock resulting in undesirable vibrations is discussed. These problems can be minimized by maintaining a hydrodynamic cushion between the button follower and the cam groove. In the present system this was achieved by utilizing a shaft seal which prevented air leakage at high rotational speeds.

INSTRUMENTATION

Instrumentation in this pilot study was devoted primarily to the measurement of blade oscillatory frequencies and flow visualization. The flow velocity in the wind tunnel was set in the conventional way from the wind tunnel test section static pressure and the total pressure and temperature measured in the plenum.

The blade oscillatory frequency was determined by one of three methods; namely, an electro-optical displacement meter, strain gages, and a cam shaft tachometer. Two proximity probes were also installed in the cam groove to provide information on cam shaft wobble. In the absence of the other signals, the output from these probes was used to determine the blade oscillatory frequency.

All methods of frequency measurement yielded identical results since the system was rigid. The only slippage that could occur was between the motor pulley and cam shaft pulley since this coupling was accomplished by means of a belt. Although direct measurements of belt slippage were not made, slippage, if any, occurred only during startup and proved to be a negligible problem.

The electro-optical displacement meter was a commercial instrument designed to measure the displacement and frequency of the vibrating blade. The instrument, which is located outside the test section, tracks a discontinuity of light reflected from the edge of the blade and converts the optical image to an electron image. A servo loop controlled the position of the electron image in an aperture. The deflection current required to keep the image cen-

tered in the aperture as the blade was oscillated became a measure of the blade displacement.

A network of two dual strain gages were attached to opposite sides of the arm connecting the blade trunnion to the cam. A conventional full bridge circuit was connected to a commercial digital strain signal processor. In this study, the absolute levels of strain were not of interest; however, it was desirable to confirm that the strain gages would remain intact while oscillating the blade and yield a clean signal from which blade oscillatory frequencies could be determined. In future applications in multi-blade facilities interblade phase angles will be measured by cross-correlation methods based on similar strain gage signals.

Signals from the optical displacement meter, strain gage signal processor, and proximity probes were preconditioned and recorded on a frequency modulated (FM) magnetic tape recorder with a frequency response from dc to 2.5 kilohertz, flat to within ±0.5 decibel. Tachometer and strain gage signals were also read on digital meters.

Frequencies were obtained from the taped signals directly by coupling the output to a digital frequency analyzer, and, in some cases, by analyzing the signal on the LeRC Omniferous Fast Fourier Transform (FFT) Analyzer. The latter method had the advantage of providing supplementary information such as the spectral content of the signal from which an indication of harmonic distortion could be obtained.

Flow visualization was accomplished by means of the double-pass Schlieren system depicted schematically in figure 4. Initial tests were performed with the off-axis system shown in figure 4(a). This was the simpler of the two systems; however, it provided a double image of the shock wave patterns in the test section as shown in figure 5. A lambda shock pattern is clearly evident; however, details of the flow near the blade surface tend to be obscured by the double image. In figure 5 the dark region located near the downstream suction surface of the blade was the result of oil vapors emanating from an oil impregnated bushing in the large trunnion (this problem was eliminated in later tests).

The double image produced by the simple off-axis system shown in figure 4(a) was eliminated by adding a beam splitter (semireflecting mirror) to the system as shown in figure 4(b). Tests with the beam splitter yielded better Schlieren images as shown in figure 6.

The Schlieren images were photographed with a 16-millimeter high-speed

motion picture camera operating at about 5000 frames per second (or about 10 frames per cycle of blade motion). A series of photographs will be presented to indicate the changes in flow pattern accompanying the oscillatory motion of the blade. However, it is generally recognized that a single frame or even a collection of single frames from high-speed motion pictures of a periodic phenomenon is an inadequate substitute for film viewed with a movie projector, since the lack of clarity in a single frame is compensated by the advantage of being able to detect motion. With this consideration in mind, the description of the flow patterns associated with a particular blade motion should be regarded as more or less typical.

A series of Schlieren photographs of the stationary blade with flow were obtained with a 35-millimeter single lens reflex camera at a shutter speed of 1 millisecond (approx 15 times slower than the effective exposure time of high-speed motion pictures at 5000 frames per second). These photographs provide a reference image for comparison with the images obtained during simulated flutter.

OPERATING CONDITIONS

The basic parameters were the Mach number, M, blade mean angle of attack, $\overline{\alpha}$, and the blade oscillatory frequency, f. Instrumentation parameters included the Schlieren optical arrangement (refer to fig. 4) and knife edge position. Additional parameters, associated with the development of the blade drive system, included the shaft bushing and seal configurations; however, details concerning the design of these components will be omitted.

Factors which remained constant in the tests were the blade geometry (fig. 2), and the amplitude of the blade motion during oscillation. The amplitude of blade motion was $\pm 1.2^{\circ}$ about the mean angle of attack, corresponding to a blade tip total displacement of 0.16 centimeter. It should be noted that the blade motion was determined by the cam configuration. Bench tests with two other cam configurations indicated that the blade could be driven at frequencies comparable to those reported herein with tip total amplitudes of 0.08 and 0.32 centimeter or $\pm 0.6^{\circ}$ and 2.4°, respectively.

The ranges of operating conditions for the present tests are summarized in table I. Two Mach numbers are shown in table I; namely, a reference Mach number M_{ref} and a free-stream Mach number M_{∞}. These Mach numbers were calculated from wall pressures measured at the positions shown in the

sketch in table I. Differences in M_{ref} and M_{∞} occurred because of the blockage effects of the blade coupled with compressibility effects associated with the formation of shock waves on the blade. The greatest differences between M_{ref} and M_{∞} occurred at the largest angles of attack and highest velocities. The reference Mach number was held fixed in the tests so, consequently, the upstream Mach number differed slightly as the blade angle of attack was varied. Both M_{ref} and M_{∞} will be given in the figures.

The main purpose of table I is to show the range of possible combinations of parameters that were feasible. Obviously, tests could have been performed at lower values of velocity and blade oscillatory frequency; however, emphasis was placed on limit testing since ultimate use of the system will be for subsonic stall flutter simulation.

An attempt was made to systematically vary the parameters and obtain high-speed motion pictures of Schlieren images at each test condition. However, good quality pictures were not always obtained (for one reason or another). Since the number of possible parametric combinations of operating conditions was large, many of the tests were not repeated. Therefore, only the results from tests yielding the best quality flow visualization will be presented. These results were from tests near the upper limits of operation shown in table I.

RESULTS

Blade Torsional Resonance

In order to maintain two-dimensional motion during oscillation, experience indicated that it was necessary to design the blade so that the first torsional natural frequency exceeded the desired frequency by a few hundred hertz. As the first natural frequency was approached, the blade began to twist as shown typically in figure 7 for an early double-wedge stainless steel blade. This twisting motion was accompanied by high stresses in the driven end of the blade attachment region.

Early stainless steel blades of the type shown in figure 7 had a first torsional natural frequency of about 700 hertz and failed at about 550 hertz. The first natural torsional frequency for the present titanium blade was determined from calculations based on a lumped parameter method and from a laser speckle interfrometer and time-averaged holography. Details of the

calculations will be omitted; however, the results from the two methods agreed within about 10 percent - the calculations yielded slightly higher values of natural frequency. The convenience and simplicity of the experimental approach made it somewhat more desirable for determining the resonance characteristics of the blade.

In the speckle interfrometer arrangement, the blade was mounted vertically with the large trunnion clamped tightly in a heavy strap and massive support. The small trunnion was supported in a clamp and rubber bushing thus permitting rotation at the free end. Blade excitation was provided by means of an audio oscillator and speaker located directly behind the blade at midspan. The location of the source was not a critical factor in determining the natural frequencies of the blade. The support system exhibited a natural frequency at about 250 hertz which was far below the range of interest. Therefore, coupling of this resonance frequency with the blade natural frequency could be neglected.

Fringe patterns of the blade first torsional natural frequency of 932 hertz are shown in figure 8. The lack of symmetry in the pattern was believed to be the result of the support system rather than blade imhomogenities. Blade stresses could be estimated from these fringe patterns; however, the calculations were not performed because the results depended on the excitation amplitude (output of the loudspeaker). A direct simulation of the stress pattern associated with torsional oscillation of the blade in the wind tunnel appeared infeasible since the amplitudes during the wind tunnel tests were appreciably greater.

Oscillatory Motion Away from Resonance

Harmonic distortion. - A measure of the distortion in the blade tip motion is the harmonic distortion function, Ψ, where

$$\Psi = \left(\frac{\overline{e_2^2} + \overline{e_3^2} + \ldots \overline{e_n^2}}{\overline{e_1^2} + \overline{e_2^2} + \ldots \overline{e_n^2}} \right)^{1/2} \tag{1}$$

In equation (1), the value of $\overline{e_n^2}$ represents the mean-square-amplitude at the n^{th} harmonic and $\overline{e_1^2}$ represents the amplitude at the first harmonic or fundamental frequency. An FFT analysis of the signals from a proximity probe

located over the blade tip in bench tests indicated that the harmonic distortion through the second harmonic was only 0.012 or 1.2 percent at a blade oscillatory frequency of 600 hertz. In the wind tunnel tests, using the signal from the optical displacement meter focused on the end of the blade containing the small trunnion, the harmonic distortion ranged from 1.5 to 3.3 percent through the fourth harmonic for frequencies between 600 and 750 hertz. A photograph of a typical signal from the optical displacement meter is shown in figure 9 for a frequency of 660 hertz. The corresponding amplitude spectra for this signal are shown in figure 10. The harmonic distortion for this case was 3.3 percent through the fourth harmonic. The amplitude of the second harmonic, at 1.3 kilohertz, was nearly 30 decibels less than the fundamental as shown in figure 10.

Steadiness and repeatability. - Normal run times were about 30 seconds with a minimum of 10 seconds at steady flutter conditions. The amount of frequency drift in a given test ranged from 2 to 5 hertz or less than 1 percent of the operating frequency. The drift was always in the direction of increasing frequency and was attributed primarily to heating of the lubricant surrounding the cam and follower.

Repeatability of the oscillatory conditions was generally within 4 hertz (less than 1 percent of the operating frequency) after the first run. At the highest frequency of 767 hertz, differences in frequency of up to 15 hertz could occur between the first "cold" run and second run in a given day. This initial difference in frequency could often be reduced or eliminated by initiating a short "break in" run prior to data acquisition.

Flow Over Stationary and Oscillating Blade

A series of Schlieren photographs of the flow over the stationary blade are presented in figure 11. The photographs were taken at $\overline{\alpha} = 3^\circ$, 4°, and 5° and at reference Mach numbers of 0.75 and 0.79. These photographs reveal the presence of an increasingly strong shock with increasing $\overline{\alpha}$ and/or Mach number. Lambda shocks are clearly visible at $\overline{\alpha} = 4^\circ$ and 5° when $M_{ref} = 0.79$ (figs. 11(e) and (f)). These shock patterns closely resemble those shown in references 11 and 12 for curved airfoils.

In all of the photographs except the one corresponding to $\overline{\alpha} = 5^\circ$ and $M_{ref} = 0.75$ (fig. 11(c)), the upper and lower boundary layer wakes appear as parallel white lines. A similarity in the appearance of these wakes would be expected if the boundary layer remained attached to both surfaces. After

boundary-layer separation on the suction surface, reattachment could occur downstream of the normal shock and the wakes would appear to be similar. However, it is not clear that this was the case because the large trunnion shadow extended over much of the region just downstream of the normal shock. For example, in figure 11(f) ($\overline{\alpha} = 5^{\circ}$, $M_{ref} = 0.79$) the boundary layer may not not have reattached, thus resulting in a thick free shear layer which would not be as visible in the Schlieren photographs as the shed vorticity in the boundary layer.

Selected sequences of frames from the high-speed motion pictures of the airfoil flutter motion were reproduced and enlarged and are presented in figures 12 to 16. The instantaneous angle of attack was determined from a knowledge of the oscillatory frequency, the framing rate of the movie camera, and the upper and lower limits of the angle of attack (e.g., when $\overline{\alpha} = 4^{\circ}$, $2.8^{\circ} \leq \alpha \leq 5.2^{\circ}$). By observing the direction of blade motion on a frame-by-frame basis and matching the direction of observed motion with an assumed motion over approximately 50 frames, a resolution of about $\pm 0.02^{\circ}$ could be obtained at a speed of 4200 frames per second and blade oscillatory frequency of 650 hertz. At a speed of 3240 frames per second and blade oscillatory frequency of 650 hertz, the resolution was $\pm 0.15^{\circ}$ after 30 frames. This seemingly tedious method of determining the blade instantaneous position was simplified by performing the matching of assumed and actual blade motion on a computer. Subsequent output was used to select frames at specific values of α.

The results in figures 12 to 16 are for $0.75 \leq M_{ref} \leq 0.79$, and $661 \leq f \leq 767$ hertz. These conditions correspond to a nominal reduced frequency Ω of $0.69 \leq \Omega \leq 0.78$ where

$$\Omega = \frac{\pi f c}{U_{\infty}} \tag{2}$$

These relatively high reduced frequencies are within the range where subsonic torsional stall flutter occurs in turbomachinery. However, simulating these high reduced frequencies coupled with large torsional amplitudes and high loading is not commonplace. Usually high reduced frequencies are obtained by oscillating the blade at low frequencies ($\approx$100 Hz) and low velocities (often in the incompressible flow regime) and/or by using large chord blades thus necessitating low torsional frequencies. Figures 12 to 16 show some of the qualitative features of the flow over an oscillating blade operating simultaneously at high

subsonic Mach numbers, high reduced frequencies, and high torsional amplitudes and loading.

The photographs in figure 12 were obtained at a simulated flutter frequency of 655 hertz and reference Mach number of 0.79. The blade was oscillated $\pm 1.2^{\circ}$ about the mean angle of attack of 4°. The cyclic appearance and disappearance of a normal shock wave is apparent. In several of the photographs, especially during the upward portion of the cycle, flow separation appears to occur near the leading edge (figs. 12(c) to (e) and (i)). On the downward stroke, the normal shock forms and the separated flow becomes more diffuse, possibly disappearing or reattaching in the region of the trunnion shadow.

A large hysteresis effect is also apparent with the motion of the flow lagging the motion of the blade. This lag becomes more apparent when viewing the motion pictures; however, an indication of this lag can be obtained by comparing the flow patterns in figures 12(f) and (g) with the pattern in figure 12(i). The latter photograph was obtained at approximately the mean angle of attack during upward movement of the blade whereas in figures 12(f) and (g) the blade is moving down. Extensive shock patterns, which were apparent during the downward motion, disappeared during the upward motion. This is quite apparent in figure 13, which represents the blade at approximately the mean angle of attack on the downward stroke (fig. 13(a)) and the upward stroke (fig. 13(b)).

The photographs in figure 14 are also for a mean angle of attack of 4° and an oscillatory frequency of 661 hertz; however, the reference Mach number is slightly lower ($M_{ref} = 0.75$). Separation appears to be more evident than it was in figure 13. Again, the large phase lag can be noted by comparing photographs with comparable angles of attack on the downward and upward strokes.

The photographs in figure 15 correspond to a mean angle of attack of 4° and a reference Mach number of 0.79 as in figure 12. However, the flutter frequency was increased to 767 hertz which represents the highest frequency for the present series of tests. Here the shock waves are quite pronounced with normal shocks extending out of the field of view (e.g., figs. 15(c) and (b)). Flow separation is apparent in most of the photographs. The phase lag appears to be quite large at this frequency. For example, the normal shock attains its maximum downstream position (approx the 1/3 chord point) at an angle of attack of about 3.5° (figs. 15(a) and (e)). Also, the shock waves appear less extensive at high angles of attack (e.g., figs. 15(d) and (h)). In these latter photographs a weak forward-moving shock appears near the 2/3 chord position.

The last series of photographs, presented in figure 16, were obtained at a mean angle of attack of 2°, an oscillatory frequency of 662 hertz, and a refer-

ence Mach number of 0.75. At this lower value of $\overline{\alpha}$, shock formations are not apparent; however, a phase lag can still be detected.

A quantitative assessment of the phase lag observed in figures 12 to 16 can be obtained from the motion pictures of the Schlieren images. In this investigation it was convenient to define this phase lag as the difference between the time the blade attains its maximum angle of attack and the time required to attain the maximum downstream normal shock position. The phase lag, as defined in this manner, is not the same phase lag discussed, for example, in reference 3. In the latter case, the definition of phase lag was based on measurements of the force coefficients on the blade and represents the classical interpretation of phase lag associated with flutter.

The phase lag determined from the flow visualization results can be described mathematically by first considering the following expression for the instantaneous angle of attack, α, of a blade oscillating in simple harmonic motion:

$$\alpha = \overline{\alpha} + \theta_0 \cos \omega t \tag{3}$$

where $\overline{\alpha}$ is the mean angle of attack, and θ_0 is the amplitude of oscillation. The maximum angle of attack α_m is

$$\alpha_m = \overline{\alpha} + \theta_0 \tag{4}$$

and the value of α_s, where the normal shock attains its maximum downstream position, is

$$\alpha_s = \overline{\alpha} + \theta_0 \cos \Phi \tag{5}$$

The phase angle Φ relating α_m and α_s was obtained from the Schlieren motion pictures.

The photographs in figure 12 suggest that at $\alpha_s \approx 4.5^\circ$ (fig. 12(f)), the shock is probably near its maximum downstream position (also compare with fig. 11(c) for steady-state flow over the blade at $\overline{\alpha} = 5^\circ$). Actually, many frames of moving picture film have to be analyzed to determine the maximum downstream position of the shock pattern. Such an analysis indicated the value of α_s for the data in figure 12 was 4.2°. Substitution of α_s into equation (5) along with $\overline{\alpha} = 4^\circ$ and $\theta_0 = 1.2^\circ$ yields a phase angle Φ of 80°. The oscillatory frequency for this case was 655 hertz ($\Omega = 0.66$). Results from the films for other runs indicated a trend of increasing phase lag with increasing

reduced frequency as shown in figure 17. A least squares linear fit of the data through the origin indicated that

$$\Phi(\text{radians}) = 2.18\,\Omega \tag{6}$$

for the limited conditions of this study. While this phase angle (based on shock position) may not be significant or sufficiently general for use in current stall flutter analysis, it reflects the kind of aerodynamic phase lag occurring at realistic flutter frequencies.

REMARKS

The results of the present study provide a qualitative picture of the flow over an isolated airfoil oscillating at frequencies associated with subsonic torsional stall flutter in fans and compressors. Although the present results do not provide a data base from which analytical models for stall flutter can be developed, they do suggest an experimental approach to this ultimate goal. It has been shown that (1) metal blades mounted in a high subsonic wind tunnel can be driven at controlled frequencies and amplitudes consistent with subsonic stall flutter and (2) a double-pass Schlieren system can be satisfactorily operated in the system.

Application of the mechanical, high-speed torsional drive mechanism coupled with the optical system to a multiblade linear cascade appears to be feasible. In a cascade arrangement, the desired number of barrel cams (equal to the number of blades) would be mounted on a common drive shaft. Control of the interblade phase angles could be obtained by adjusting the relative angular positions of the cams. Phase angle monitoring during oscillation can be obtained by cross-correlation of strain gage signals from the cam follower arms.

The system described in this report is not necessarily limited to the simulation of subsonic torsional stall flutter conditions. However, since these conditions constitute an extreme environment for the system in terms of the oscillatory frequencies and blade loading requirements, the system should be capable of operating in other simulated flutter regimes. The principal compromise associated with the mechanical drive system is the dynamic testing time which is nominally 10 to 20 seconds. However, this operating time is generally adequate for most data acquisition needs.

SUMMARY OF RESULTS

A novel mechanical drive system for oscillating blades in torsion at frequencies up to 767 hertz and amplitudes of $\pm 1.2^{\circ}$ has been described. This system operates in a nonresonant mode and, consequently, requires a much higher power input than would be required in a resonant system. The primary advantage of the nonresonant mechanical system is that the amplitude of oscillation can be predetermined.

High-speed motion pictures of Schlieren images of the flow over an oscillating blade at reduced frequencies in the range of 0.52 to 0.78 revealed rather extensive shock patterns at free-stream Mach numbers of about 0.7 and a mean angle of attack of 4°. A phase lag resulting from the slow response of the flow to the motion of the blade was particularly evident while viewing the motion pictures. This phase lag resulted from the difference between the time the blade attained its maximum angle of attack and the time required for the normal shock to reach its maximum downstream position. The phase angle increased with increasing reduced frequency, reaching a maximum value of about 100° at the above operating conditions.

REFERENCES

1. Sisto, F.; and Perumal, P. V. K.: Lift and Moment Prediction for an Oscillating Airfoil with a Moving Separation Point. ASME Paper 74-GT-28, Mar. 1974.

2. Arnoldi, R. A.; et al.: Analytical and Experimental Study of Subsonic Stalled Flutter. Pratt and Whitney Aircraft, July 1977. (AFOSR-77-0854TR, AD-A043127.)

3. Sisto, F.; and Ni, Ron Ho: Research on the Flutter of Axial-Turbomachine Blading. Tech. Rep. ME-RT-72005, Stevens Institute of Technology, May 1972.

4. Gray, L.; Liiva, J.; and Davenport, F. J.: Wind Tunnel Tests of Thin Airfoils Oscillating Near Stall. Vol. I. Summary and Evaluation of Results. D8-0925-1, Vol. 1, Boeing Co., 1969. (USAAVLABS TR 68-89A.)

5. Whitehead, D. S.: Force and Moment Coefficients for Vibrating Aerofoils in a Cascade. R&M No. 3254, British A.R.C., 1962.

6. Carta, F. O.; and St. Hilaire, A. O.: An Experimental Study on the Aerodynamic Response of a Subsonic Cascade Oscillating Near Stall. SQUID-TR-UTRC-R76-912270. United Technologies Research Center, 1976.

7. Fleeter S.; et al.: An Experimental Determination of the Unsteady Aerodynamics in a Controlled Oscillating Cascade. ASME Paper 76-GT-17, Mar. 1976.

8. Rothbart, Harold A.: Cams. John Wiley and Sons, Inc., 1956.

9. Neklutin, C. N.: Mechanism and Cams for Automatic Machines. American Elsevier Pub. Co., Inc., 1969.

10. Hrones, John A.: An Analysis of the Dynamic Forces in a Cam-Driven System. Trans. ASME, vol. 70, no. 5, July 1948, pp. 473-482.

11. Lindsey, W. F.; Daley, Bernard N.; and Humphreys, Milton D.: The Flow and Force Characteristics of Supersonic Airfoils at High Subsonic Speeds. NACA TN 1211, 1947.

12. Stack, J.: Compressible Flows in Aeronautics. J. Aeronaut. Sci., vol. 12, no. 2, Apr. 1945, pp. 127-148.

TABLE I. - NOMINAL OPERATING CONDITIONS

Total pressure, N/cm^2 abs	9.86
Total temperature, K	297
Reynolds number based on chord, Re_c	1×10^6
Reference Mach number*, M_{ref}	0.61 to 0.79
Free-stream Mach number*, M_∞	0.58 to 0.72
Mean angle of attack, $\overline{\alpha}$, deg	0 to 4
Oscillatory amplitude, θ_0, deg	±1.2
Oscillatory frequency, f, Hz	492 to 767
Reduced frequency, $\Omega = \pi fc/U_\infty$	0.52 to 0.78

*Refer to sketch.

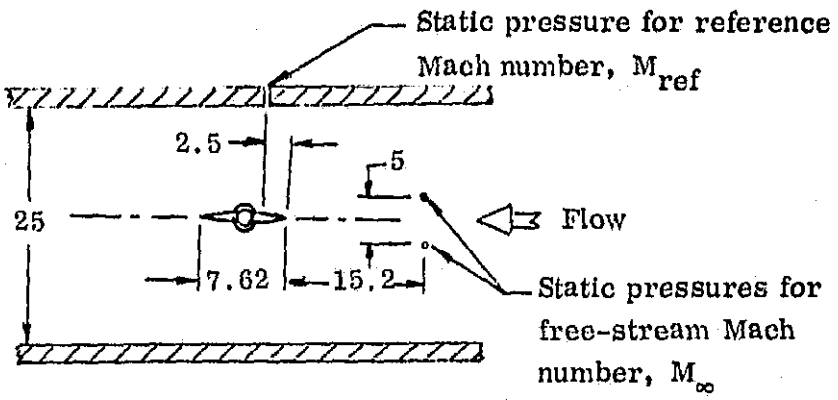

Location of test section reference and free-stream static pressures.
All dimensions in centimeters.

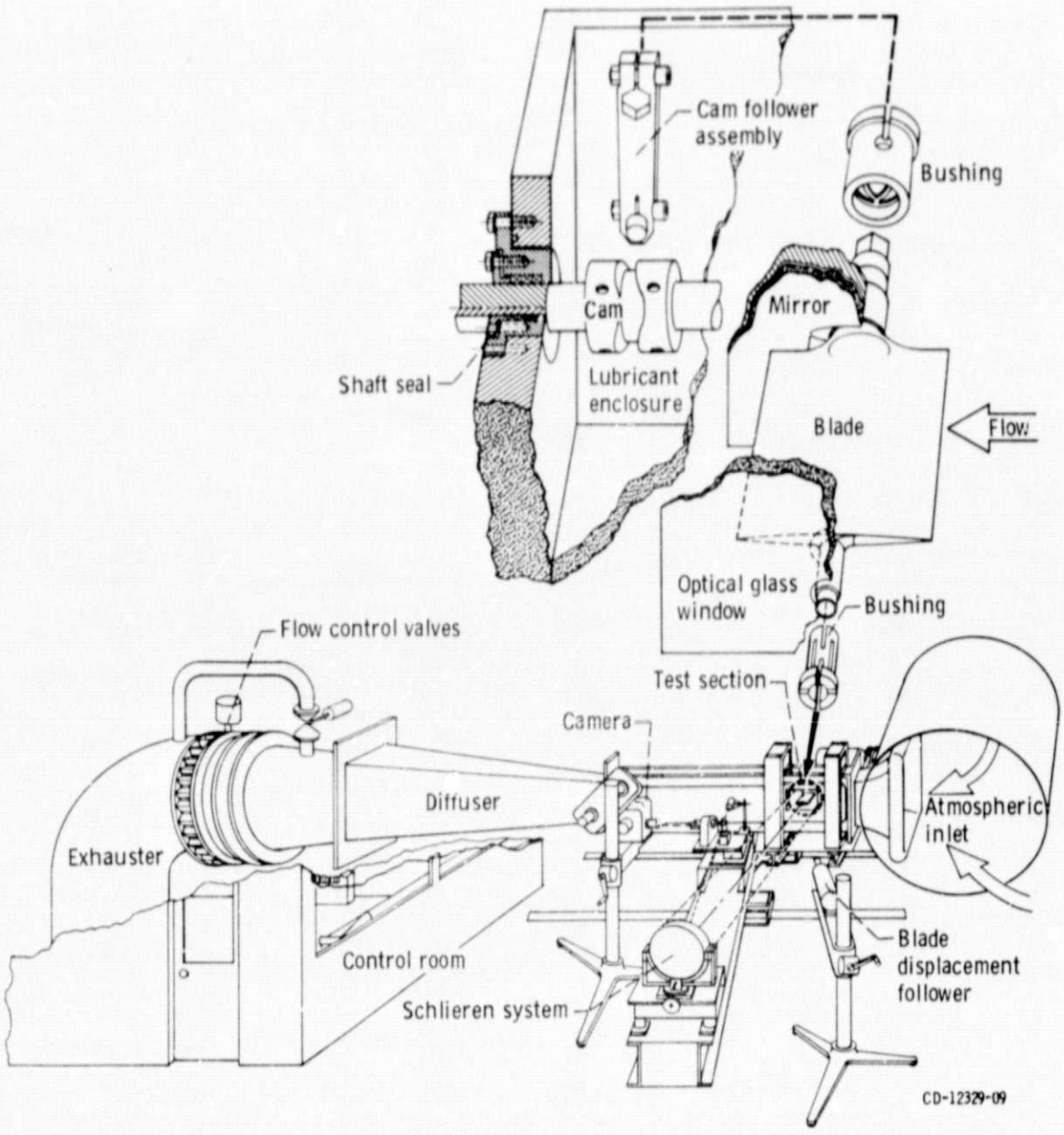

Figure 1. - Flutter test facility.

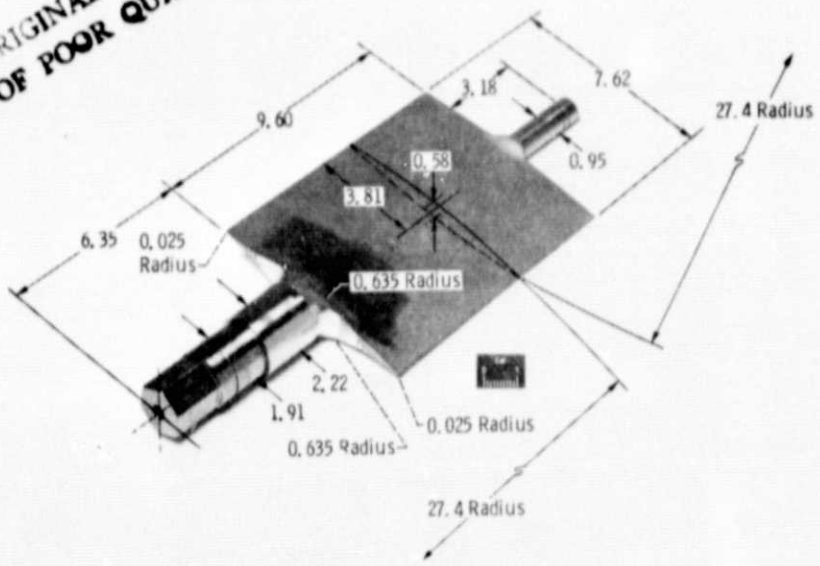

Figure 2. - Titanium flutter blade. (All dimensions in centimeters.)

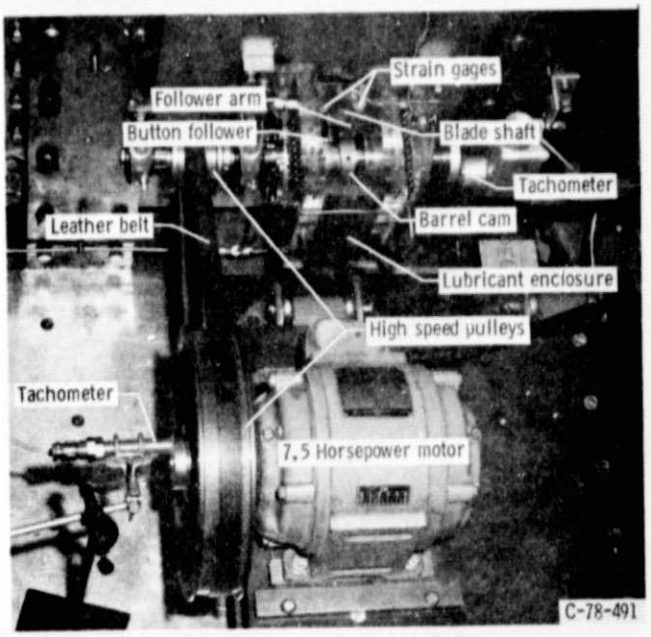

Figure 3. - Blade oscillatory drive system.

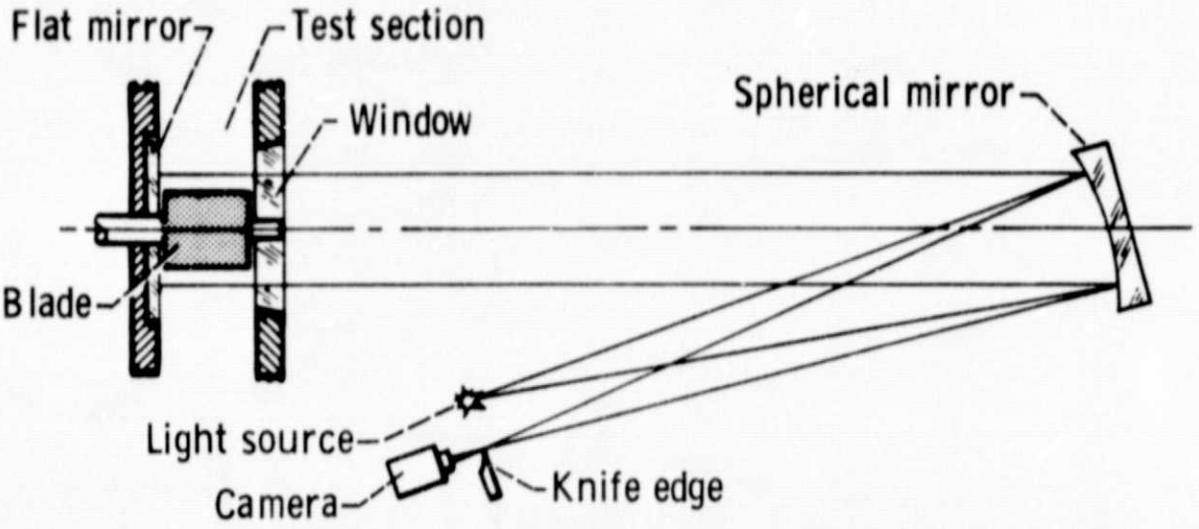

(a) Original system without beam splitter.

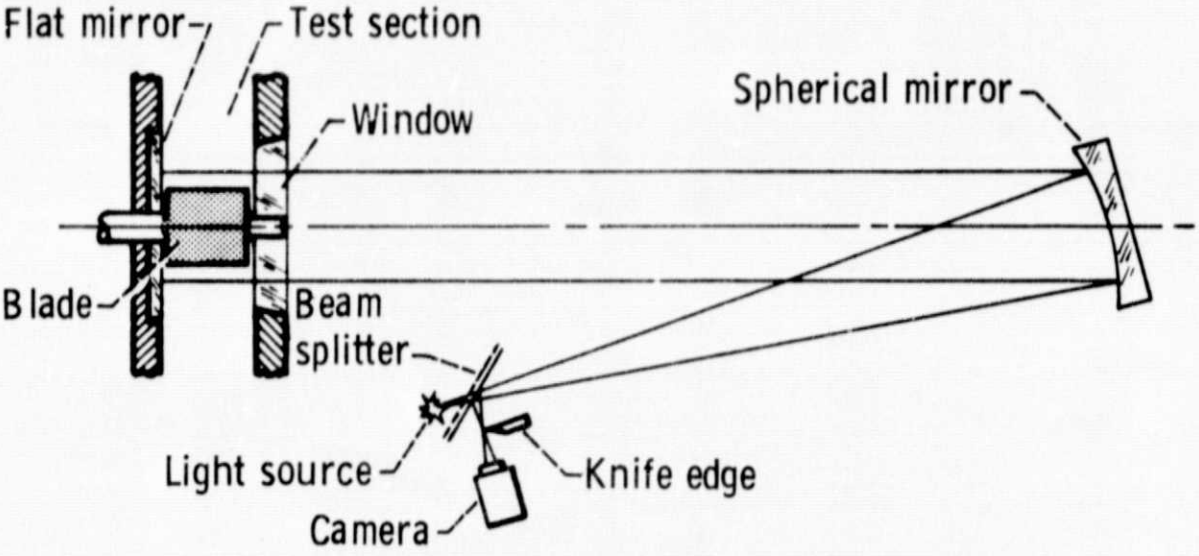

(b) Current system incorporating a beam splitter.

Figure 4. - Double-path Schlieren systems used in flutter tests.

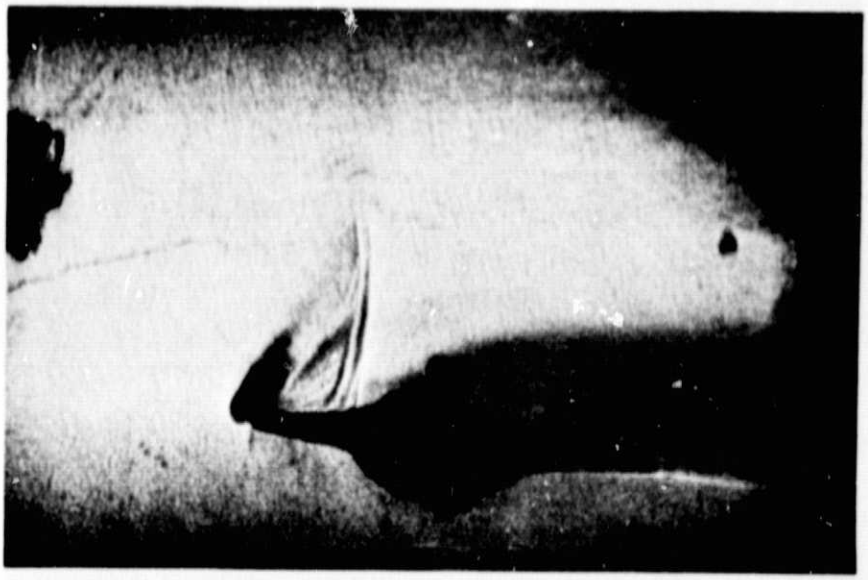

Figure 5. - Photograph from a single frame of high speed motion picture film showing double-image of shock pattern from optical system shown in figure 4(a).

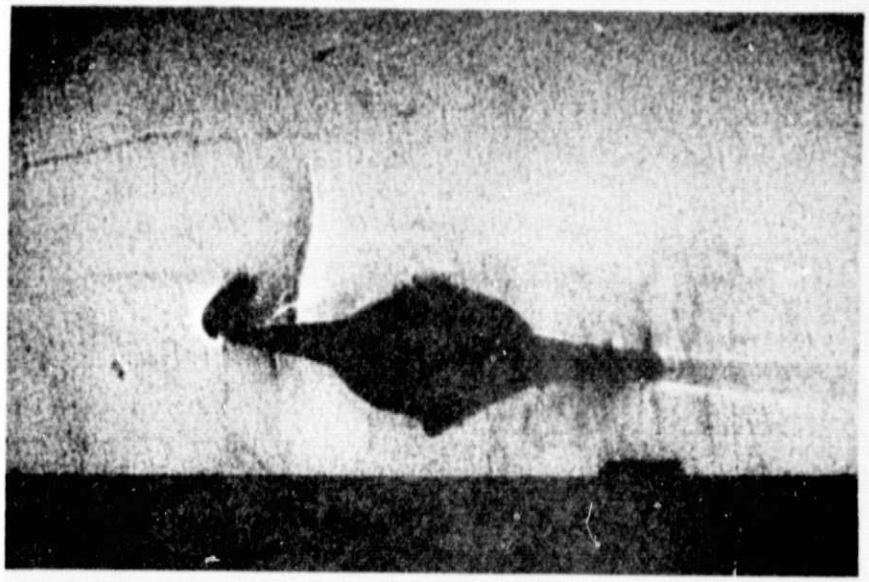

Figure 6. - Photograph from a single frame of high speed motion picture film showing shock pattern from optical system shown in figure 4(b) (includes beam-splitter).

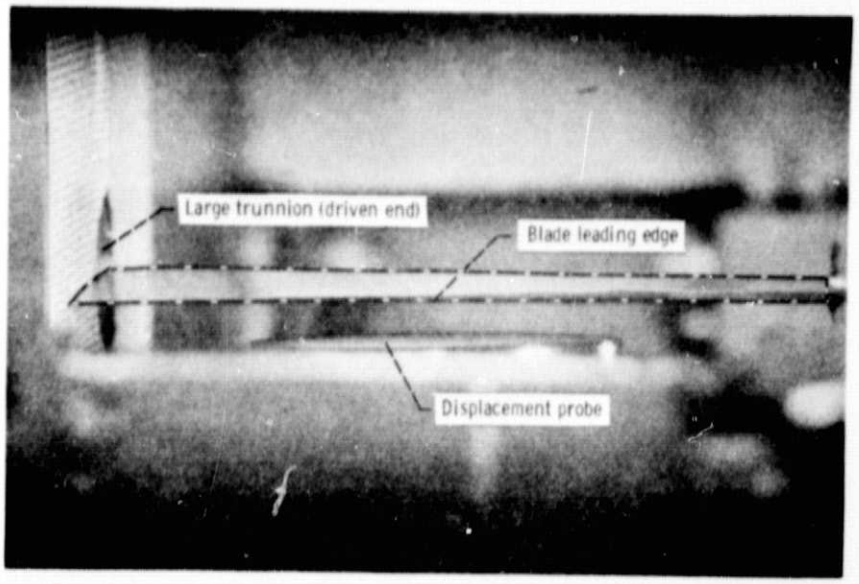

(a) Twist near top of pitching motion.

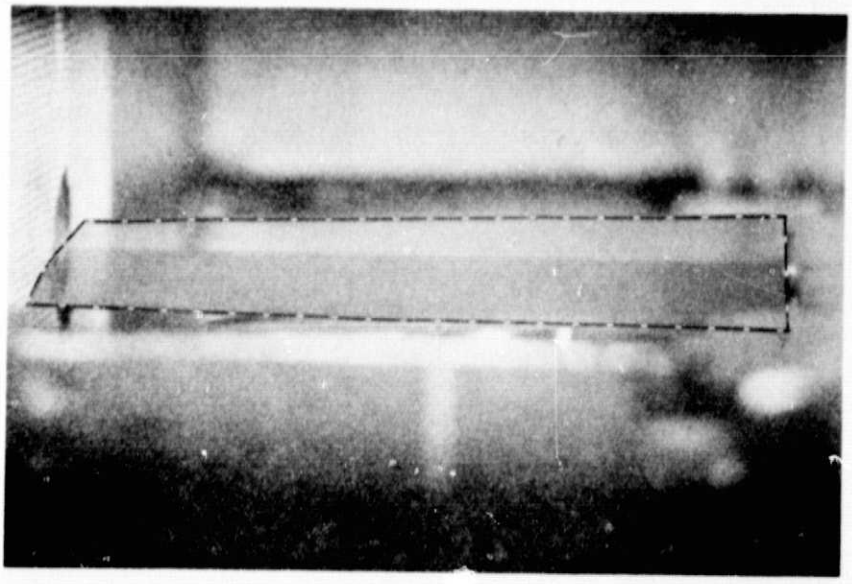

(b) Twist near bottom of pitching motion.

Figure 7. - Twisting motion of double-wedge blade oscillating near resonance in the absence of flow.

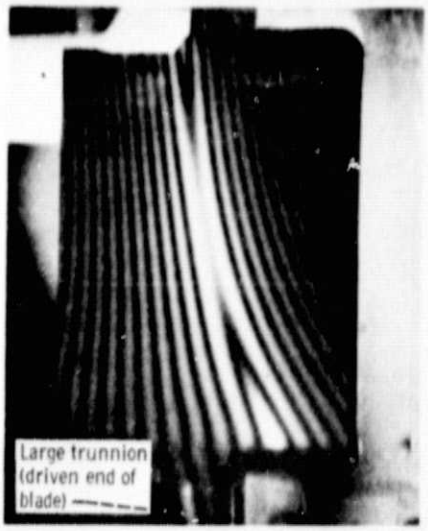

Figure 8. - Fringe pattern at blade first torsional natural frequency of 932 Hertz.

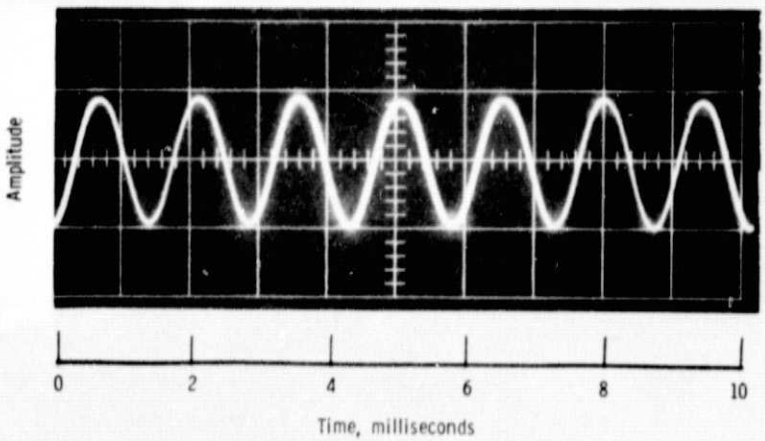

Figure 9. - Signal from optical displacement meter showing blade tip motion at an oscillatory frequency of 660 Hertz.

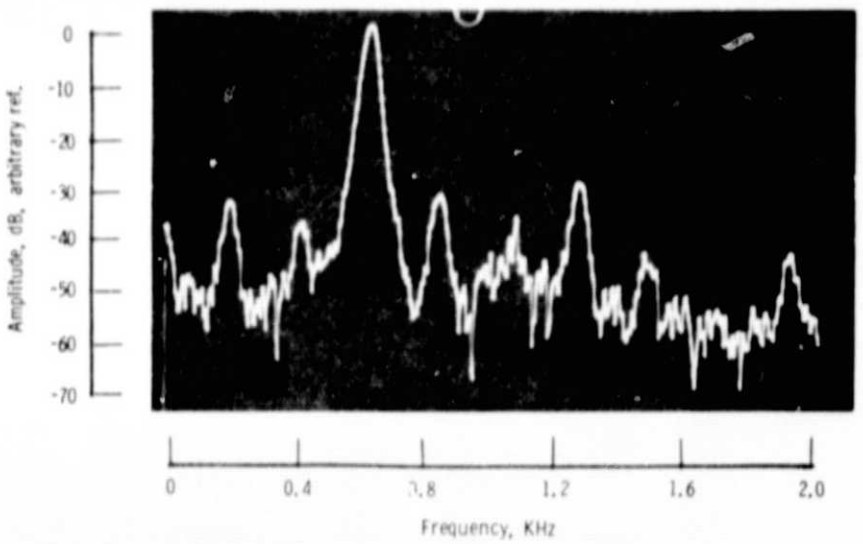

Figure 10. - Narrow-band (30 Hz) spectra of blade displacement signal (figure 9) for an oscillatory frequency of 660 Hertz.

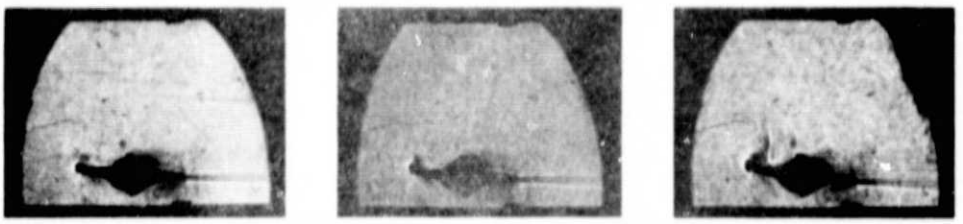

(a) $\bar{\alpha} = 3^0$; $M_{ref} = 0.75$; $M_{\infty} = 0.71$. (b) $\bar{\alpha} = 4^0$; $M_{ref} = 0.75$; $M_{\infty} = 0.69$. (c) $\bar{\alpha} = 5^0$; $M_{ref} = 0.75$; $M_{\infty} = 0.67$.

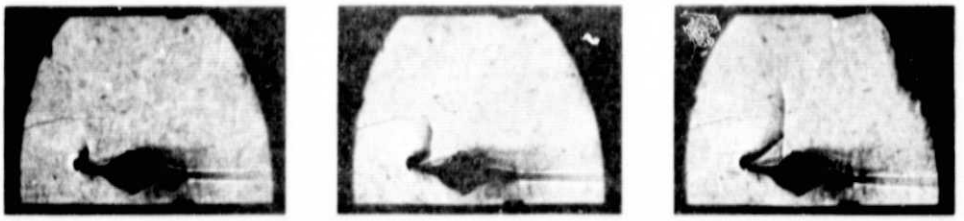

(d) $\bar{\alpha} = 3^0$; $M_{ref} = 0.79$; $M_{\infty} = 0.75$. (e) $\bar{\alpha} = 4^0$; $M_{ref} = 0.79$; $M_{\infty} = 0.72$. (f) $\bar{\alpha} = 5^0$; $M_{ref} = 0.79$; $M_{\infty} = 0.70$.

Figure 11. - Flow patterns over stationary blade.

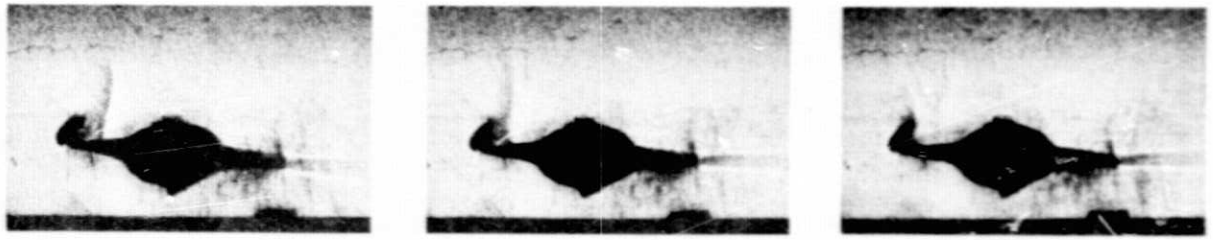

(a) $\alpha = 4.56^0$, pitching down.

(b) $\alpha = 3.59^0$, pitching down.

(c) $\alpha = 2.98^0$, pitching down.

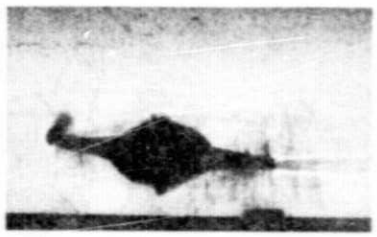

(d) $\alpha = 3.95^0$, pitching up.

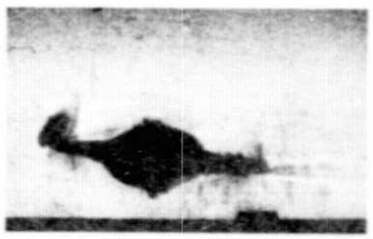

(e) $\alpha = 4.92^0$ pitching up.

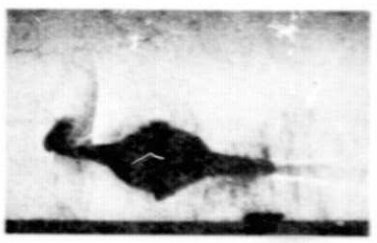

(f) $\alpha = 4.51^0$, pitching down.

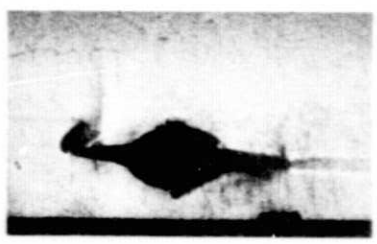

(g) $\alpha = 3.54^0$, pitching down.

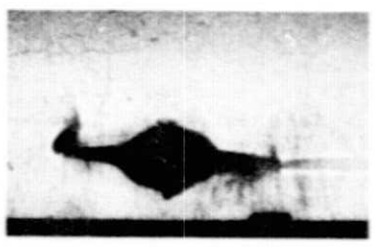

(h) $\alpha = 3.03^0$, pitching up.

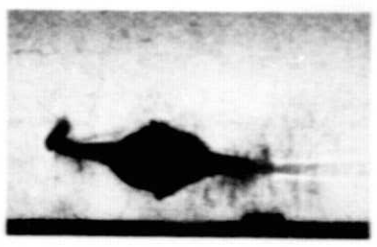

(i) $\alpha = 4.00^0$, pitching up.

Figure 12. - Flow patterns over oscillating blade. Mean angle of attack $\bar{\alpha} = 4^0$; instantaneous angle of $2.9^0 \leq \alpha \leq 5.2^0$; oscillatory frequency $f = 655$ Hz; reference Mach number $M_{ref} = 0.79$; free stream Mach number $M_\infty = 0.72$; reduced frequency $\bar{\Omega} = 0.66$.

(a) Downward pitching motion; $\alpha = \bar{\alpha} = 4^0$.

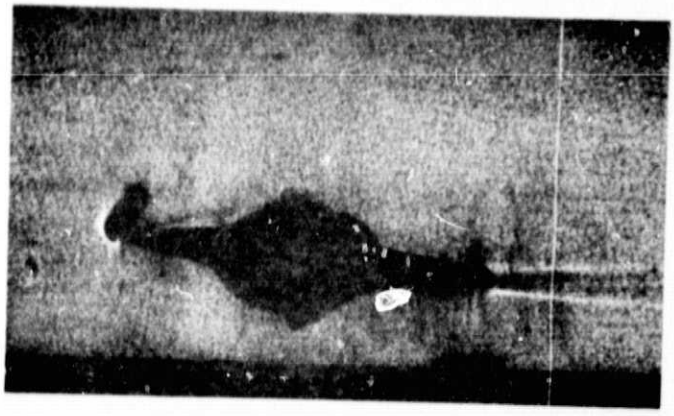

(b) Upward pitching motion; $\alpha = \bar{\alpha} = 4^0$.

Figure 13. - Flow patterns during upward and downward pitching motion at the mean angle of attack of 4^0. Oscillatory frequency, $f = 655$ Hz; reference Mach number, $M_{ref} = 0.79$; free stream Mach number, $M_\infty = 0.72$; reduced frequency, $\Omega = 0.66$.

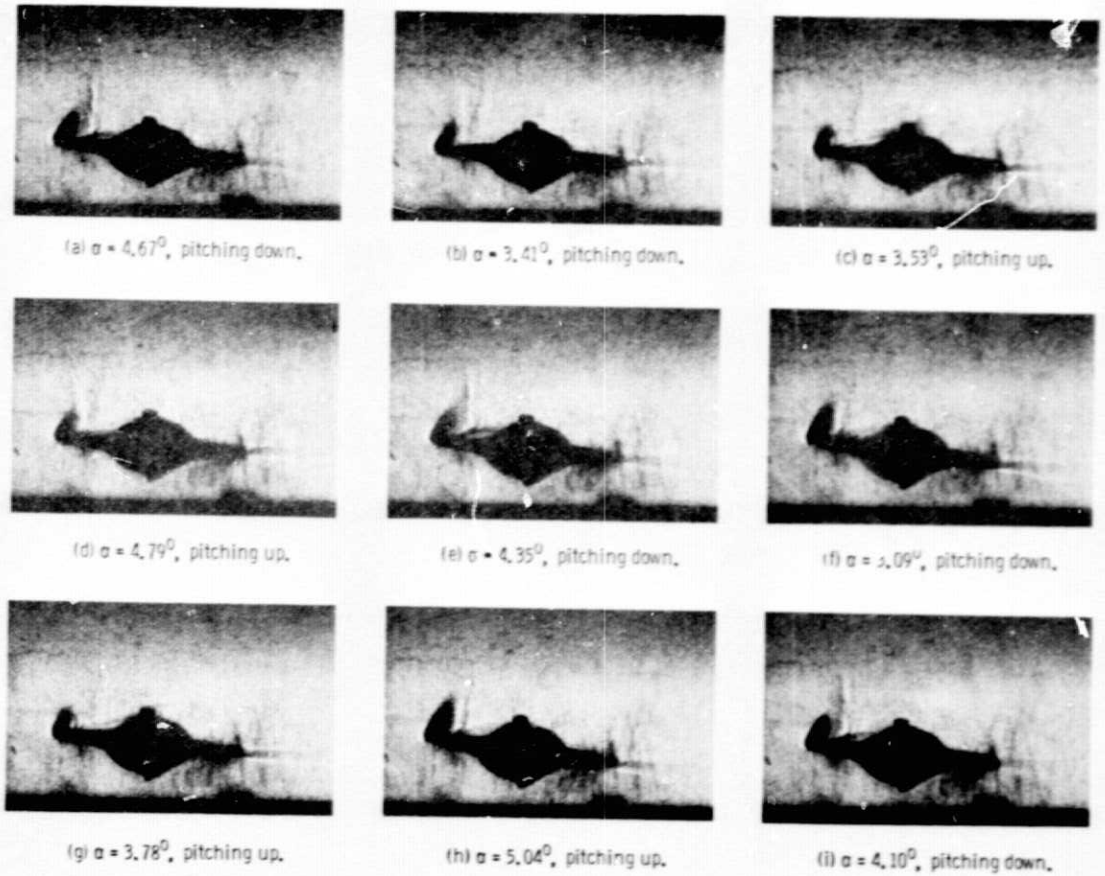

(a) $\alpha = 4.67^0$, pitching down. (b) $\alpha = 3.41^0$, pitching down. (c) $\alpha = 3.53^0$, pitching up.

(d) $\alpha = 4.79^0$, pitching up. (e) $\alpha = 4.35^0$, pitching down. (f) $\alpha = 3.09^0$, pitching down.

(g) $\alpha = 3.78^0$, pitching up. (h) $\alpha = 5.04^0$, pitching up. (i) $\alpha = 4.10^0$, pitching down.

Figure 14. - Flow patterns over oscillating blade. Mean angle of attack $\bar{\alpha} = 4^0$; instantaneous angle of attack $2.8^0 \leq \alpha \leq 5.2^0$; oscillatory frequency f = 661 Hz; reference Mach number $M_{ref} = 0.75$; free stream Mach number $M_\infty = 0.69$; reduced frequency $\Omega = 0.69$.

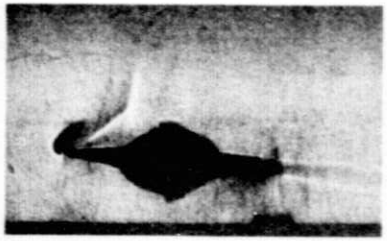

(a) $\alpha = 3.41^0$, pitching down.

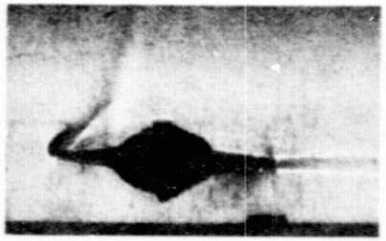

(b) $\alpha = 3.37^0$, pitching up.

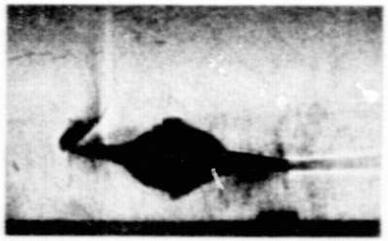

(c) $\alpha = 4.55^0$, pitching up.

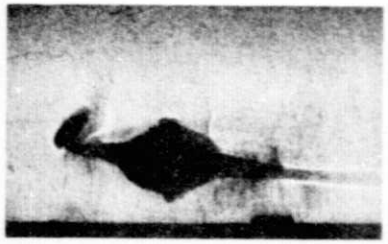

(d) $\alpha = 4.67^0$, pitching down.

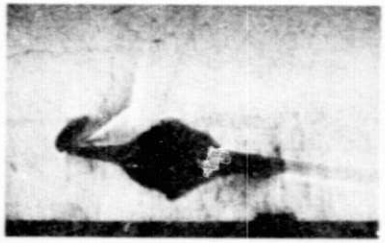

(e) $\alpha = 3.49^0$, pitching down.

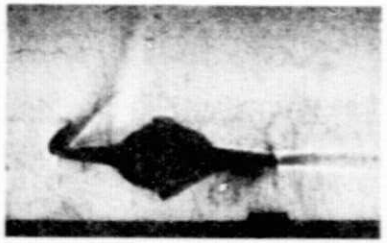

(f) $\alpha = 3.29^0$, pitching up.

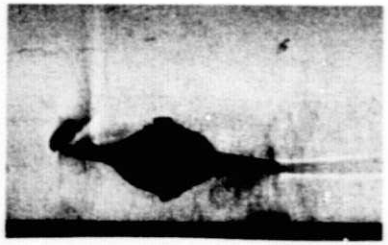

(g) $\alpha = 4.47^0$, pitching up.

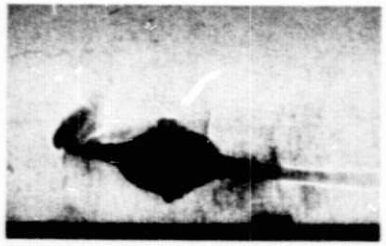

(h) $\alpha = 4.75^0$, pitching down.

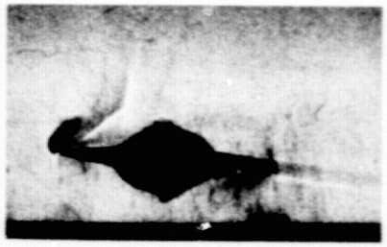

(i) $\alpha = 3.57^0$, pitching down.

Figure 15. - Flow patterns over oscillating blade. Mean angle of attack $\bar{\alpha} = 4^0$; instantaneous angle of attack $2.8^0 \leq \alpha \leq 5.2^0$; oscillatory frequency f = 767 Hz; reference Mach number $M_{ref} = 0.79$; free stream Mach number $M_\infty = 0.72$; reduced frequency $\Omega = 0.78$.

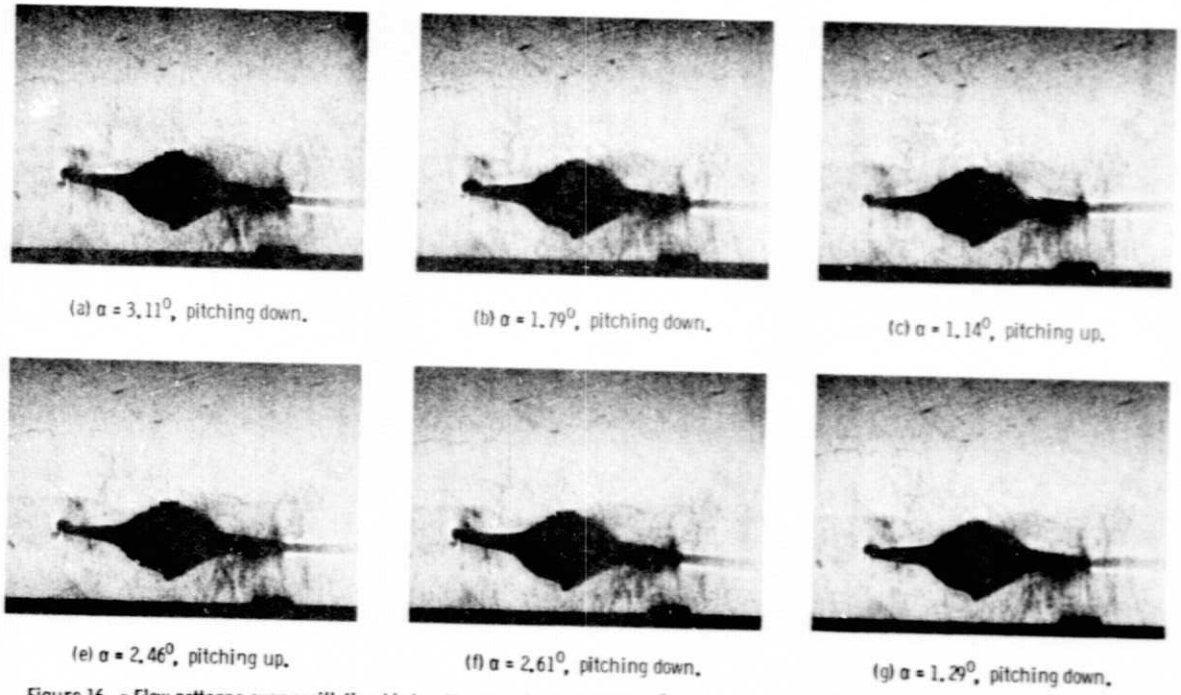

(a) $\alpha = 3.11^{0}$, pitching down.

(b) $\alpha = 1.79^{0}$, pitching down.

(c) $\alpha = 1.14^{0}$, pitching up.

(e) $\alpha = 2.46^{0}$, pitching up.

(f) $\alpha = 2.61^{0}$, pitching down.

(g) $\alpha = 1.29^{0}$, pitching down.

Figure 16. - Flow patterns over oscillating blade. Mean angle of attack $\bar{\alpha} = 2^{0}$; instantaneous angle of attack $0.8 \leq \alpha \leq 3.2^{0}$; oscillatory frequency f = 662 Hz; reference Mach number $M_{ref} = 0.75$; free stream Mach number $M_{\infty} = 0.69$; reduced frequency $\Omega = 0.69$.

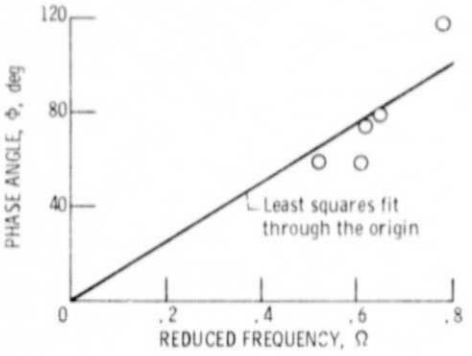

Figure 17. - Approximate variation of phase angle with reduced frequency for $\bar{\alpha}$ = 4 deg and θ_0 = 1.2 deg.